Andrzej Pacut, Adam Czajka, "Aliveness detection for iris biometrics", *2006 IEEE International Carnahan Conference on Security Technology, 40th Annual Conference, October 17-19, 2006, Lexington, Kentucky*

ALIVENESS DETECTION FOR IRIS BIOMETRICS

Paper No. ICCST-2004-

Andrzej Pacut, *Senior Member, IEEE* and Adam Czajka, *Member, IEEE*

Institute of Control and Computation Engineering
Warsaw University of Technology
Nowowiejska 15/19
00-665 Warszawa
POLAND

Research and Academic Computer Network NASK
Biometric Laboratories
Wawozowa 18
02-796 Warszawa
POLAND

e-mails: {A.Pacut,A.Czajka}@ia.pw.edu.pl

Abstract - Various experiments show an alarming lack of anti-spoofing mechanisms in devices already protecting many sensitive areas all over the world, proving that aliveness detection methods must be quickly included in commercial equipment. To introduce and systemize the topic, the paper begins with a survey of possible types of eye forgery, together with possible countermeasures. The authors introduce three solutions of eye aliveness detection, based on analyses of image frequency spectrum, controlled light reflection from the cornea, and pupil dynamics. A body of various fake (printed) eye images was used to test the developed methodologies, including different printers and printout carriers. The proposed methodology was embedded into the NASK iris recognition system and showed its large potential. For a local database of pairs of alive and printed eyes, all methods proposed in the paper revealed zero False Acceptance Rate of Fakes FAR-F. The False Rejection Rate of Genuines FRR-G reached 2.8% for the first proposed solution, and showed null value for the next two proposed methods. This very favorable compares to the commercial equipment tested: two popular iris cameras accepted 73% and 15% of the prepared fake irises.

Index Terms — aliveness detection, iris recognition, biometrics

I. INTRODUCTION

The aliveness detection became a serious and disturbing issue after publishing in 2002 the experiment results done (much earlier) in the Fraunhofer Research Institute (Darmstadt, Germany) in collaboration with the German Federal Institute for Information Technology Security (BSI) [1] with well-established face, fingerprint and iris recognition systems. The experiments highlighted an alarming lack of anti-spoofing mechanisms in devices already protecting many sensitive areas all over the world. The Panasonic ET100 iris camera with PrivateID software was successfully fooled with iris printouts of high resolution (1200x2400 dpi) made with the inkjet printer. Since the ET100 camera looks for the infrared light reflection from the cornea, one needs to make a small hole instead of the pupil.

The situation became more serious, where the first systematic experiment of iris spoofing was carried out by Tsutomu Matsumoto of Yokohama National University, Japan, and presented in London in 2004 [2]. Three cameras were used in the experiment, namely OKI IrisPass-h, Panasonic Authenticam ET100 and OKI IrisPass-WG. The fake printouts were made with color laser printer, and the images were captured twofold: by way of Panasonic ET100 camera, which produces relatively poor quality iris images, and using a digital microscope equipped with an infrared illuminator. Both the enrollment and the verification stages were tested. Only IrisPass-WG did not enroll fake irises. All three tested cameras accepted the fake printouts at the verification stage. This enforced the need for aliveness detection methodology to be quickly introduced to the commercial equipment, stressed the need for the research on fake resistive iris recognition.

II. IRIS FORGERIES AND COUNTERMEASURES

A. Iris counterfeits databases

Presently, there is no publicly available databases of images (or other measurements) of iris counterfeits. Such databases are, however, essential for developing anti-spoofing methods. To prepare such a base, the printouts of eye images using different printing color depth and printout carriers were prepared for 29 volunteers at NASK. All the volunteers contributed to the *development database*, while six of them, randomly chosen, were asked for the second session of iris measurements to finally form the *evaluation database*. The base was used to test and compare the results of aliveness detection implemented in commercial equipment and those proposed in this paper. In all printouts prepared, a small hole is made in place of the pupil, as such a trick is typically sufficient for fake iris capture by commercial systems.

1) Development database

To adjust parameters of the proposed methods, we collected a development database of 569 fake eye printouts.

Most of the presented results were obtained as a part of BioSec European integrated project IST-2002-001766

The database was collected for 57 different eyes originating from all 29 volunteers. Although the iris images used are taken in the infrared light by a monochrome camera, it is suggested [2] to use a color laser printer to make forgeries, despite of the lack of color information within the image. We tried both variants, using laser printers working at 300 and 600 dpi resolutions. Number of prepared printouts vs. different carriers, printers and resolutions are detailed in Table I.

TABLE I
NUMBER OF IRIS PRINTOUTS FORMING THE DEVELOPMENT DATABASE.

		Printing: 300 dpi		Printing: 600 dpi	
Printer	**Carrier**	**b&w**	**color**	**b&w**	**color**
Konica Minolta C350	Regular Matt 80g/m^2	57	57		
Konica Minolta C350	Matt 90g/m^2 with foil coat	57	57		
Konica Minolta C350	Transparent foil	57	57		
Xerox WorkCentre 24	Xerox 100g/m^2 Matt			57	
Xerox WorkCentre 24	Xerox 120g/m^2 Matt with foil coat			56	
Cannon IRC 3200	Mondi 200g/m^2 Matt				57
Cannon IRC 3200	Mondi 135g/m^2 Glossy				57
	Total	**342**		**227**	
		569			

Figure 1 demonstrates a few examples of the printouts created for 600 dpi resolution on three different carriers, namely a matt and glossy paper and a transparent foil. Note that each printed eye has its natural size on the printout.

Figure 1. Example printouts on different carriers (from left to right: matt paper, glossy paper and transparent foil) which were used to test the commercial equipment and anti-spoofing methods.

2) Evaluation database

Six types of iris printouts of 600 dpi resolution were prepared for 6 volunteers (i.e., for 12 different eyes) using three different carriers (matt and glossy paper as well as a transparent foil), and two printing color options: grayscale and full color. We resigned from low quality printouts of 300 dpi resolution at the evaluation stage. We also did not include foil printouts into the evaluation set, since they proved to be very resistive to the successful eye capture, both for commercial and laboratory equipment. Consequently, for each eye, three printouts for three different iris images were prepared to simulate multiple attack trials with different fake samples. Table II details the evaluation set of the prepared printouts.

TABLE II
NUMBER OF IRIS PRINTOUTS FORMING THE EVALUATION DATABASE.

Printer	**Carrier**	**Printing: 600 dpi b&w**	**Printing: 600 dpi color**
Cannon IRC 3200	Mondi 135g/m^2 Glossy	36	36
Cannon IRC 3200	Mondi 200g/m^2 Matt	12	36
Xerox WorkCentre 24	Xerox 100g/m^2 Matt	24	
	Total	**144**	

B. Vulnerability

NASK Biometric Laboratories team had repeated the Matsumoto experiments with ET100 camera, confirming the claim that ET100 is relatively easy to be fooled by simple printouts of at least 600 dpi resolution. Additionally, testing of Panasonic ET300 camera was performed, which depicted that also this camera accepts fake irises. We detail now both experiments.

For each printout forming the evaluation database, we made 10 independent attack trials, both for color and grayscale printouts, thus making 120 trials per one eye. We summarize the percentage of accepted fake irises separately for all four variants in Table III, presenting the highest and the average FAR-F obtained among three printouts used. The results show that Camera A (ET100) suffers a lack of aliveness detection, since approximately 94% of verification trials were successful for fake irises using grayscale printouts. Although it is clear that Camera B (ET300) is relatively more difficult to enforce a successful verification of counterfeits, still in average 15% of fake trials were accepted, which is frustratingly high.

TABLE III
PERCENTAGE OF FAKE EYES ACCEPTANCE BY COMMERCIAL SYSTEMS, TESTED IN NASK BIOMETRIC LABORATORIES VS. DIFFERENT CARRIERS AND PRINTOUT TYPES. TESTED CAMERAS: A – PANASONIC ET100, B – PANASONIC ET300

Carrier	Glossy: Mondi 135g				Matt: Mondi 200g + Xerox 100g			
Printing	b&w		color		b&w		color	
Printout	best	all	best	all	best	all	best	all
Camera A	94,17	86,7	66,7	58,9	93,3	72,2	80,0	73,1
Camera B	0,0	0,0	23,3	15,6	0,0	0,0	0,0	0,0

C. From eye image to actual eye

The eye printouts make a quite straightforward iris forgery. As revealed in our tests, the leading iris biometric cameras have difficulties in differentiating between the fake and alive eyes even if a low cost printout of low resolution is used as an eye imitation. We found out that eye images using other carriers like mobile phone or laptop LCD displays of sufficient resolution, were rejected due to low matching score. To complement the list of possible eye printouts, one may

imagine a special holographic image imitating spatial eyeball features.

Next step in iris forgery would be a preparation of an "eye movie", which simulates the real eye behavior (like blinks, pupil dynamics, eyeball movements, etc.). Naturally, such a movie with a fixed scenario is relatively easy to eliminate, e.g. by requesting and measuring a particular eye behavior. On the other hand, the attacker may be able to react on-line to certain requests; hence additional anti-spoofing methods must be applied.

Going further into counterfeit complexity, we may consider an artificial eye presented behind the camera lens. The iris pattern may be printed on a plastic or rubber eye model, whose constrictions and dilations may additionally imitate pupil diameter changes and a natural behavior of the iris trabecular meshwork during accommodation. Finally, the living eye may be the carrier for artificial contact lens with the iris pattern printed.

The most sophisticated "forgery" of the iris camera is simply the use of a real eye. Although the use of non-living organ may have a bit drastic tinge, this cannot be excluded with the iris biometrics increase of its strength and position in automatic authentication. At the end we reach the last possibility, namely a forced use of one's eye against owner's will. While this is very difficult to detect, we propose a pupil dynamics approach, which is hoped to also react to a level of stress while authenticating the iris. However, additional research towards a link between the pupil dynamics and our psychological state is required.

D. Countermeasures against Iris Forgery

There is a need for the iris counterfeit classification as well as for a systematic approach to the subterfuge prevention. Some issues regarding the iris aliveness were already addressed by Daugman [5,6]. Here we classify a few variants of iris counterfeits detection into several groups, characterized by the increasing level of the method sophistication.

The first group of anti-spoofing methods employs the *external eye features*. This may be realized either in a passive or in an active way. The first subgroup – *passive measurements* – relies on characteristics of the living eye as opposed to artificial objects. These may include a smoothness of the frequency spectrum typically obtained for images of live organ. The same frequency analysis reveals dominating frequencies, which may indicate that the iris image was altered in a regular way, e.g. by printing using a raster device. Increasing the measurement dimensionality, one may check the 3D eye structure, like its spherical shape. The human eyeball has a fixed and stable shape, and knowing its parameters one may employ simple reflection mechanisms to assert the 3D shape of the measured object. In turn, the *active measurements* bring a possibility to check certain eye characteristics in real time, with a limited possibility to be guessed by the attacker. This, as an example, includes the analysis of inflicted infrared light reflections from the moist cornea.

The second group of countermeasures to iris spoofing includes the methods examining the *internal eye structure*. Two Daugman's propositions may be classified into this countermeasure class, namely the analysis of the eye tissue at different wavelengths and analysis of the so called Purkinje reflections [6]. Since the melanin pigment responsible for the eye color has a specific infrared light absorption profile, this may be used to distinguish between a live tissue enriched with melanin and e.g. the glassy eye imitation free from organic elements. On the other hand, the Purkinje reflections are difficult to be observed, and typically only two out of four are clearly visible, Fig. 2. To robustly observe all four, the high quality of images, partially guaranteed by an adequate depth-of-field of the optical system, is required. All four Purkinje reflections are clearly visible on a few percent of images observed in various publicly available databases, as well as in our local database of iris images. This may prevent the method from the expected reliability.

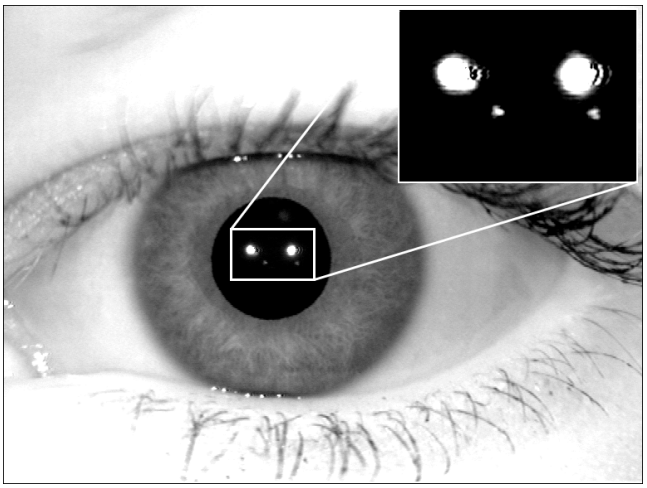

Figure 2 Example of two pairs of Purkinje reflections. The image is captured with NASK iris recognition system.

Finally, yet importantly, the third group of possible anti-spoofing mechanisms is based on *dynamic* (i.e. behavioral) *eye features*. Again, similarly to the previous group, one can perform the measurement passively or actively. It was suggested in literature [5,6] that the human pupil oscillates constantly with the approximate frequency of 0.5 Hz, even in a uniform lighting conditions. This phenomenon, called the *hippus*, is relatively easy to be *passively* measured if it is observed for an eye, Fig. 3. However, our tests disclosed that not all eyes reveal a sufficient hippus signal that might be unmistakably distinguished from the noise using the same measuring equipment as that used for iris recognition.

It seems that the dynamic features of the eye observed within certain time horizon should be a result of a certain interaction between the user and the machine. This makes the measurement *active*. The human-machine interaction may be twofold. The first, *command driven reaction*, is the consequence of the system request to perform some action by the user requesting to be authenticated. This may include blinks or eye movement forced by an object tracking. However, this kind of interaction may be uncomfortable to the user, since a supplementary training is required besides the one offered prior to the iris biometrics usage. Moreover, this kind of anti-spoofing mechanism is difficult to implement in negative identification systems, i.e. systems aiming at recognizing criminals.

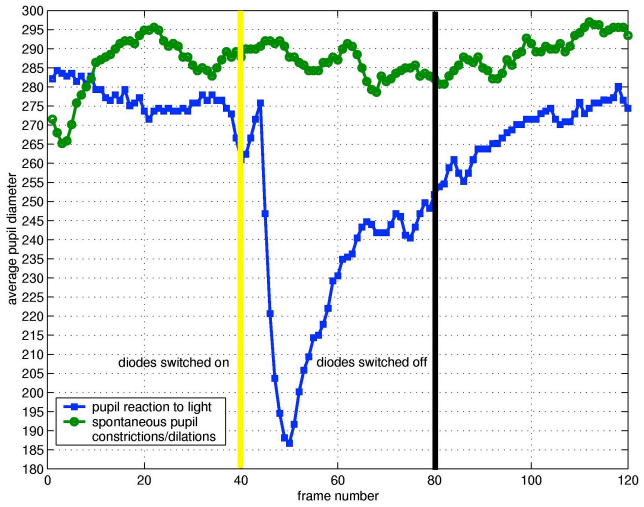

Figure 3 Example of spontaneous pupil diameter oscillation (top line) and the typical pupil diameter reaction to light changes (bottom line) [3,4]. Both measurements were obtained using NASK iris recognition system. Frames were collected every 125 ms.

Almost ideal situation is to actively measure those stimulus driven eye dynamic features which are independent of our consciousness, and are not interfering with typical iris recognition process. One of such features is the pupil dynamics. Primarily, the pupil constriction and dilation partially influences the human eye accommodation process, and is classified in psychology as the conditional response. There was a lot of research referring to this phenomenon. It is also widely used in diagnostics of certain neurological disorders. Since early 60's, there is a research aiming at modeling the pupil reflex as a control system. In 1967 Clynes and Cohn proposed [7] a model of human pupil response to step luminescence changes. The model is different for positive and negative luminescence steps, hence nonlinear. This type of models is employed in this paper even for more general light signals to develop a new automatic method of eye aliveness detection.

III. ALIVENESS DETECTION METHODS

A. *Frequency spectrum analysis (FS)*

1) Introduction: Frequency spectrum seems to be a straightforward source of information concerning the existence of regular artifacts within the image. The concept of artificial frequencies localization prior to the iris recognition was already suggested in the literature [5,6], however no automatic methodology was proposed to materialize the ideas existed for years.

Frequency spectrum methodology has an important advantage, namely, it requires no additional hardware, since the same static image as used in the iris recognition may be analyzed. On the other hand, the method has a serious drawback, originating from Shanon's theory. Namely, the method fails once the resolution of the printing device, used for counterfeit preparation is more than twice the resolution of the analysis camera.

Additional question arises, which part of the image should be analyzed. The obvious aim is to take as large area as possible, to average the noise and expose the artificial frequencies. On the other hand, we aim at detection of fake irises, thus fake eyelids, eyelashes or fake skin is out of our interest. Consequently, the proposed method was tested for two variants of analysis areas, namely the 256x256 rectangle centered at the pupil center (variant FS-A), and two rectangles of 64x64 pixels, located equidistantly below the pupil to minimize the chance of eyelid coverage (variant FS-B), Fig. 4. Note that both variants intentionally make use of the area dimensions to be a power of 2, which enables to employ the FFT algorithm.

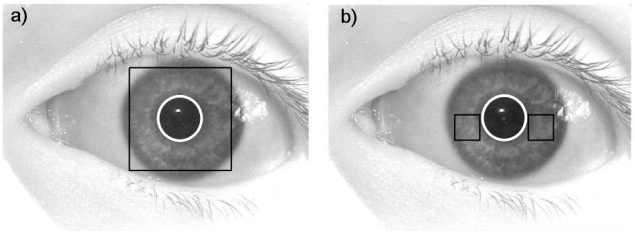

Figure 4 Two areas considered in iris frequency analysis: a) the rectangle 256x256 pixels centered at the pupil center (FS-A variant), b) two iris sectors 64x64 pixels each placed equidistantly below the pupil center to minimize the occlusion probability (FS-B variant)

2) Automatic artificial frequency recognition: To assess the level of artificial frequencies, which are the consequence of a limited printer resolution, the frequency ranges which discriminate between the printed area and the live tissue must be defined. The intuition gives a few straightforward solutions:

a) Find such a range of frequencies, starting from, and not including, the DC component, which gives the best differentiation between spectra for fake and alive irises, in terms of the percentage of spectrum contained within the defined range.

b) Just the reverse of a), fix the amount of spectrum and find such a range of frequencies (starting from the DC component) which maximally differ for alive and fake iris spectra.

c) Apply the approach a) but for a selected frequency window that does not start from the DC component.

The routine c) has one degree of freedom more when compared to a) and b). Nevertheless, it is more selective in frequency domain and it revealed in the experiments a higher accuracy than the methods a) and b). We now briefly detail this winning approach.

The method consists of two steps. The first step uses alive-counterfeit iris pairs to experimentally determine a frequency range $f_{opt} - s_{opt} < |f| < f_{opt}$, where s_{opt} is the frame width responsible for a frequency selectiveness ratio. For a given f_{opt} we calculate the percentage z_{opt} of the overall amplitude spectrum included in the defined spectrum range. We consequently chose f_{opt} to maximize the difference of z_{opt} for images of alive and fake irises. Note that f_{opt} may be different for each alive-fake image pair, thus we take the most frequent value. Once f_{opt} is fixed, the second step of the method is to find the threshold value z_{opt}^{thr} that separates distributions of z_{opt} obtained for images of alive and fake

irises. Calculations with various values of s_{opt} and employing the development database, brought us to the optimal method parameters: s_{opt} = 16, f_{opt} = 59 and z_{opt}^{thr} = 0.10 for FS-A variant, and s_{opt} = 5, f_{opt} = 12 and z_{opt}^{thr} = 0.11 for FS-B variant. Figures 5 and 6 illustrate the distributions of z_{opt} for FS-A and FS-B variants, respectively.

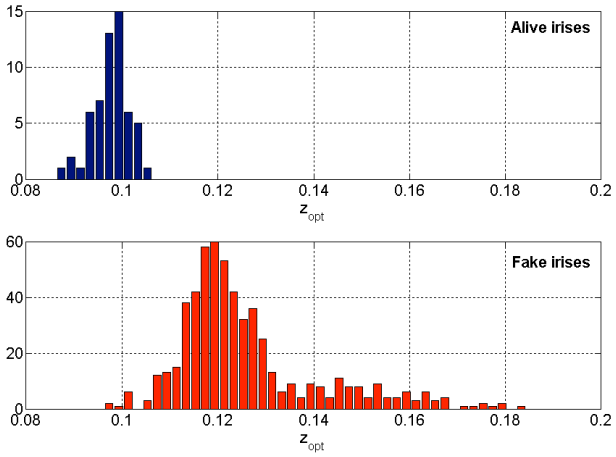

Figure 5 The distributions of the percentage z_{opt} of spectra included into the frequency range $f_{opt} - s_{opt} < |f| < f_{opt}$, for alive (top) and fake (bottom) irises in FS-A variant.

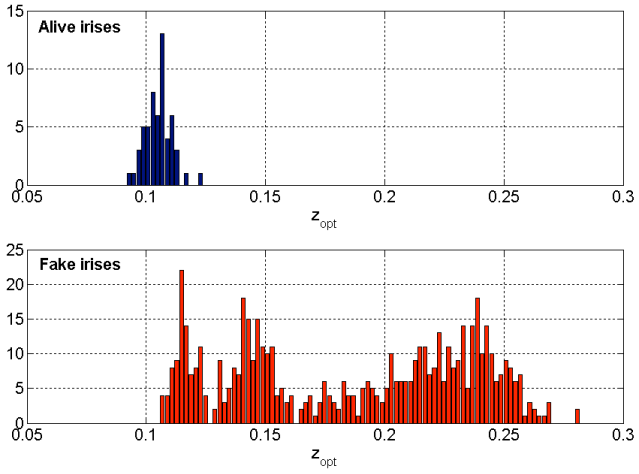

Figure 6 The same as in Fig. 5 for FS-B variant.

B. *Controlled light reflection analysis (CLR)*

1) Introduction: The idea of stimulated light reflection analysis is derived from the assumption of the eyeball spherical shape and the cornea moistness. To implement the method, the iris recognition device was extended with two supplementary NIR diodes, placed horizontally and equidistantly to the camera lens. This results in four possible reflection states, which may be observed when the iris is captured, Fig. 7 (additional central reflection is clearly visible as an effect of already existed infrared illuminator implemented for iris recognition purposes). One, however, can imagine rather arbitrary number K of supplementary illuminators, set on and off randomly, thus generating 2^K possible states.

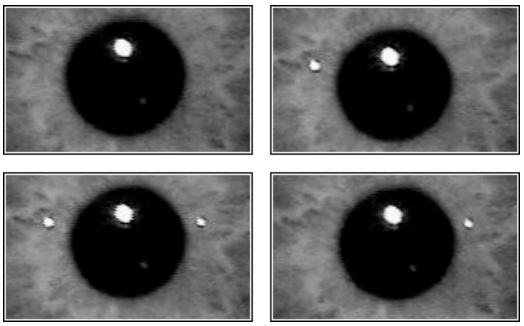

Figure 7. Four possible states of infrared stimulated reflections observed for the developed setup.

Although the number of diodes is arbitrary, the position of reflections should be chosen carefully. Note that the commercial devices accept fake images with a hole in place of the pupil, thus reflections within the pupil do not improve the aliveness detection accuracy. Moreover, to stimulate the reflections, one should select the eyeball regions that are unlikely to be covered by eyelids and eyelashes, since only then the reflections can be observed. Thus, a horizontal and relatively far (20 cm) positioning of the diodes from the lens is suggested.

2) Detection of the reflection state: The stimulated reflections are expected on both sides of the pupil, as shown in Fig. 7. Thus, the pupil must be first localized. For this purpose, we use the pupil detection method employed in our iris recognition system [8,9], however, any pupil detection mechanism may be applied here, e.g. [10,11,12]. To eliminate the outlines of the iris, where the moist cornea connects with the eyelid, the imaged is cropped to the rectangle defined by the quadruple: (x_0-4R,y_0-2R), (x_0+4R,y_0-2R), (x_0+4R,y_0+2R) and (x_0-4R,y_0+2R), where (x_0,y_0) and R is the localized pupil center and radius, respectively. This prevents from other reflections to interfere with the actual reflection map.

Once the region of interest (ROI) is determined, a filtering must be applied to detect the reflections. The Laplacian of Gaussian filtering gives positive results here, since once the filter is tuned properly, it is sensitive to particular shapes, like the specular reflections we search for. The histogram of the filtered image is normalized and the image is transformed into the binary form. This directly gives the positions of the reflections. The binarization threshold is set at the middle between the average and maximum values, independently for each normalized image.

The resulting binary image is then transformed into the vector H of sums of pixel intensities in vertical directions, for instance

$H =$

[0 0 0 0 423 550 1101 0 0 0 0 0 0 742 832 1238 0 0 …]

reflection reflection

Non-zero elements of H form partitions. Each partition in H is then represented as an element of H' representing the detected reflections, and each element of H' is characterized by the overall sum of partition member values. Thus H' consists of the values representing the position (in the

horizontal direction) and the strength of reflections. In our example we obtain:

$$H' = [0\ 2074\ 0\ 2812\ 0\ ...\ ]$$

Consequently, the detected *i*-th state of reflections is coded by way of three bits using *H*'. This results in a three-bit code *L*':

[010] – there is only one non-zero value in *H*'
(none of the supplementary diodes lights)
[011] – there are two non-zero values in *H*' and the first one is higher than the second
(left supplementary diode lights)
[110] – there are two non-zero values in *H*' and the first one is lower then the second
(right supplementary diode lights)
[111] – there are three non-zero values in *H*' and the one in the middle is the highest one
(both supplementary diode light)
[000] – entire *H*' is zero, there are more than three non-zero values in *H*', or the iris image was rejected during the pupil localization phase.

2) Measurements

Each measurement of the eye and the printouts forming the development database uses 8 random combinations of states of two supplementary diodes. Identically as for the detected diode states, the requested states are coded by three bits, forming a reference code *L*. Note that the subsequent moments of particular diode switches are, theoretically, unknown and invisible to the user. The measurements take 2 sec., and run parallel to the iris image capturing for the recognition purposes. For each given state, the vectors *L* and *L*' are compared using XOR operation. To classify the iris as a live object, the minimum number of corresponding states in *L* and *L*' was experimentally set to four. This threshold results in zero FAR-F and zero FRR-G for the development database. Figure 8 illustrates the method concept.

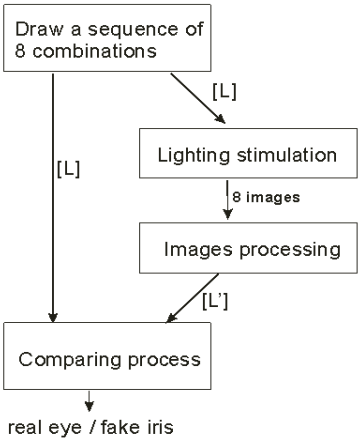

Figure 8 The scheme of stimulated infrared reflection aliveness detection routine.

C. Pupil dynamics analysis (PD)

1) Dynamics modeling

Pupil response to a step light change proposed in [7] consists of two independent channels, defined by transfer functions, whose sum gives the final response, Fig. 9. The bottom channel contains first order inertia with a lag element. This channel represents long-term, persistent response to luminescence changes. After the step stimuli occurs, this channel answers by setting a new size of pupil diameter with speed according to time constant T_3.

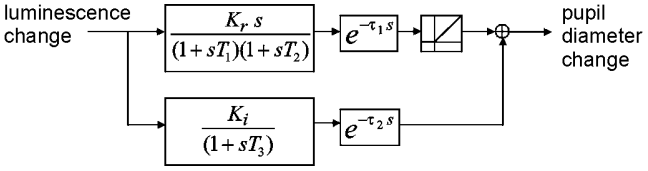

Figure 9 A dynamic model of human pupil response to step light changes by Manfred Clynes and Michael Kohn [7]

The upper channel contains second order inertia with differentiation and a lag element, and is active only for positive luminescence changes (from dark to light). This channel represents the transient response of the pupil. After the positive stimuli has occurred, the answer of this channel increases and then decreases to the zero-level with respect to T_1 and T_2 time constants. The constants K_r and K_i are negative to force the negative response for positive input.

This model explains observed phenomena, like asymmetry of the pupil constriction and dilation processes. Figure 10 shows the example response of the model fitted to the actual pupil diameter measurement. The dashed line is the response of the transient part of the model (the upper channel), the dotted line is the response of the persistent part (the bottom channel), while the ragged line is the sum of both channels, i.e. the model output.

2) Measurements

Each volunteer contributing to the development database looked into the camera lens, identically as during the iris enrollment or verification procedures. The system waits for 4 seconds to guarantee a stabilization of pupil just after the accommodation process. The LED is then lighten-up and the acquisition starts. We recorded 25 frames per second (i.e. a frame comes every 40 ms) and the acquisition time was set experimentally to 4 seconds. This is sufficient to observe the entire pupil reaction to light changes. The experiments were carried out in a real environment, i.e. we admitted a variety of external light intensity as it is typical within the office conditions.

We have used different LEDs with light ranging from red to yellow, to investigate both its potential influence on the pupil reaction modeling, as well as to check volunteer comfort. Experiments revealed that diodes emitting the white light resulted in the most distinct pupil reactions.

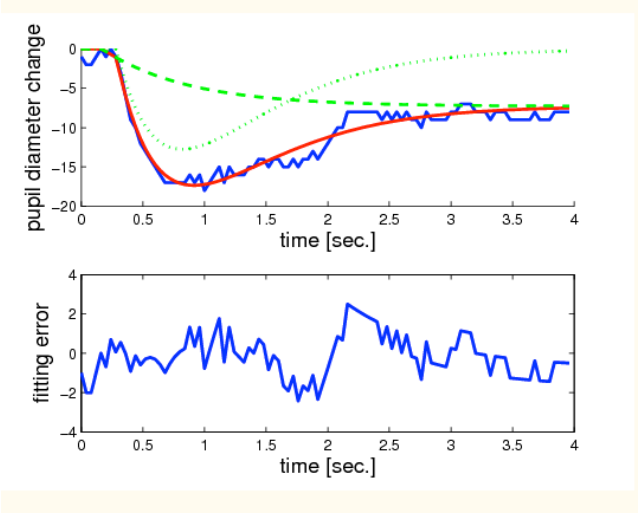

Figure 10 (top) Example of model output fitted to the experimental data. Dotted lines represent responses of the corresponding channels, while the solid line is the model output. Ragged line represents the actual measurement of the pupil diameter. (bottom) The difference between model response and the actual measurement.

3) *Feature extraction*

The measurements result in a time series representing changes in the pupil diameter. To differentiate between the alive and fake objects, we define the aliveness features as a collection of the model parameters, namely T_1, T_2, T_3, τ_1, τ_2, K_r and K_i. Features are extracted by finding the best fitting of the model output to each experimental data series. Well known methodology of model fitting may be applied here.

4) *Classification*

The last stage of the routine is to differentiate which values of the extracted features correspond to the alive iris, and which should represent measurements of a counterfeit. A two-layer nonlinear perceptron with tangent activation functions in both the hidden and output layers is used as a classifier that separates the feature vectors. One neuron is set at the output, and the network is trained to response -1 and +1 for fake and alive samples respectively. A tolerance of 0.2 is acceptable when recognizing the eye aliveness, i.e., the network response must be at least 0.8 to classify an object as a genuine eye, and below -0.8 to recognize the iris counterfeit. Network with 20 hidden neurons successfully recognized all alive and fake eyes within the development database.

For our data, the most distinguishable features are K_r and K_i which correspond to the gain of the channels. This is related to the fact that for counterfeit images, only noise values were registered. Consequently, for small stimuli or high background luminescence the network could classify real eyes as counterfeits, contributing to high values of FRR-G. The effect of low pupil reaction due to a high level of external light cannot be neglected by the system developer.

IV. RESULTS

To test the proposed methods, we used the testing protocol identical as for commercial devices, namely the same office conditions and the same number of attack trials. All parameters of the commercial systems were set to the default values, recommended by the manufacturer. A part of the evaluation database was used, namely these printout types for which the commercial equipment revealed non-zero FAR-F, as shown in Table III.

Our tests show (Table IV) that for frequency spectrum method (FS-B variant), controlled light reflection (CLR), and pupil dynamics (PD) no fake irises were accepted (zero FAR-F). Also, CLR and PD showed null rejection rate for alive irises (zero FRR-G), while FS-B has 2.8% FRR-G. Although the FS-A approach did not reject the alive irises, it accepted counterfeits, yet at the rate lower than for commercial systems.

TABLE IV
PERCENTAGE OF ACCEPTED SAMPLES FOR DIFFERENT ANTI-SPOOFING MECHANISMS. CAMERA A – PANASONIC ET100, CAMERA B – PANASONIC ET300

	Fake samples	Alive samples
FS-A	11,1	100,0
FS-B	0,0	97,2
CLR	0,0	100,0
PD	0,0	100,0
Camera A	73,1	100,0
Camera B	15,6	100,0

V. CONCLUSIONS

The proposed iris aliveness detection methods showed their high potential. We investigated three methods based on analysis of frequency spectrum (FS), controlled light reflection (CLR), and pupil dynamics (PD), using a body of various fake (printed) eye images. The limited accuracy of the FS method may be compensated by their important advantage of no additional hardware requirements, since they share the same iris image with authentication. On the other hand, implementation of the two remaining methods within the existing equipment is neither complicated nor costly. The authors suggest a procedure that joins all three proposed methods, especially for more sophisticated forms of iris counterfeit, e.g. non-living real eye.

VI. REFERENCES

[1] Lisa Thalheim, Jan Krissler, and Peter-Michael Ziegler, “Biometric Access Protection Devices and their Programs Put to the Test”, c't 11/2002, page 114 – Biometrie, available on-line at http://www.heise.de/ct/english/02/11/114/

[2] Tsutomu Matsumoto, “Artificial Fingers and Irises: importance of Vulnerability Analysis”, 7th International Biometrics 2004 Conference and Exhibition, London, UK, 2004

[3] Andrzej Pacut and Adam Czajka, “Iris Aliveness Detection”, BioSec 2nd Workshop, Brussels, January 20, 2005

[4] Heikki Alisto *et. al.*, “Biometric Modalities and Technology”, BioSec 4nd Workshop, Brussels, November 28-29, 2005

[5] John Daugman, “Countermeasures against Subterfuge", in: Jain, Bolle, Pankanti, Biometrics: Personal Identication in Networked Society, Amsterdam: Kluwer, Sec. 8, Ch. 5, pp. 103-121, 1999

[6] John Daugman, “Anti-spoofing Liveness Detection”, available on-line at http://www.cl.cam.ac.uk/users/jgd1000/countermeasures.pdf

[7] Manfred Clynes and Michael Kohn, “Color dynamics of the pupil”, Annuals of N.Y., Academy of Science, Vol. 156, 1967

[8] Adam Czajka and Andrzej Pacut, “Zak's transform for automatic identity verification”, Proceedings *of the 4th International Conference on Recent Advances in Soft Computing RASC2002, 12-13 December 2002, Nottingham, United Kingdom,* pp. 374-379, 2002

[9] Andrzej Pacut, Adam Czajka, and Przemek Strzelczyk, "Iris biometrics for secure remote access", in: J.S. Kowalik et al. (Eds.), Cyberspace Security and Defense: Research Issues, pp. 259-278, Springer, 2005

[10] John Daugman, “How Iris Recognition Works”, IEEE Transactions on Circuits and Systems for Video Technology, Vol. 14, No. 1, January 2004

[11] Li Ma, Tieniu Tan, Yunhong Wang, and Dexin Zhang, “Efficient iris recognition by characterizing key local variations”, Image Processing, IEEE Transactions on, Vol. 13, Issue 6, pp. 739 - 750, June 2004

[12] C. Sanchez-Avila, R. Sanchez-Reillo, “Two different approaches for iris recognition using Gabor filters and multiscale zero-crossing representation”, Pattern Recognition, 38 (2005), pp. 231 – 240, Elsevier 2005

VII. VITA

Andrzej Pacut, Ph.D, D.Sc. - received his M.Sc. in Control and Computer Engineering in 1969, Ph.D. in Electronics in 1975, and D.Sc. in Control and Robotics in 2000. Since 1969 he is with Warsaw University of Technology, being a Professor in the Institute of Control and Computation Engineering. Since 1999 he is with Research and Academic Computer Network NASK. He was Visiting Prof. at the Lefschetz Center for Dynamic Systems at Brown University, Providence, Rhode Island 1980–1981, and Visiting Prof. in the Department of Electrical and Computer Engineering of Oregon State University, Corvallis, Oregon, 1986-1991. He is a senior member of the IEEE, a member of INNS, and serves as the President of the IEEE Poland Section. He is a member of the NASK Research Council and the head of the NASK Biometric Laboratories.

Adam Czajka, Ph.D. - received his M.Sc. in Computer Control Systems in 2000 and Ph.D. in Control and Robotics in 2005 from Warsaw University of Technology. Since 2003 he is with Warsaw University of Technology, and since 2002 with Research and Academic Computer Network NASK. He is a member of the IEEE and serves as the Secretary of the IEEE Poland Section. He is a member of the NASK Research Council.

VIII. ACKNOWLEDGEMENTS

Authors thank Rafal Babicki for his help in preparation of the eye printouts databases and in the evaluation of frequency-based approach. The authors are also indebted Marcin Chochowski for his evaluation of pupil dynamics approach.